

Modeling of ZnO nanorods for evanescent field optical sensors

Sandra Börner^{*1}, Christian E. Rüter¹, Tobias Voss², Detlef Kip¹, and Wolfgang Schade¹

¹ Institute of Physics and Physical Technologies, Clausthal University of Technology, Leibnizstr. 4, 38678 Clausthal-Zellerfeld, Germany

² Institute of Solid State Physics, University of Bremen, P.O. Box 330440, 28334 Bremen, Germany

Received 16 March 2007, revised 27 April 2007, accepted 4 May 2007

Published online 10 July 2007

PACS 07.07.Df, 42.25.Bs, 78.20.Bh, 78.66.Hf, 78.67.–n

The optical wave guiding properties of ZnO nanorods are simulated and studied in detail using a block-iterative frequency-domain method and the results of a finite difference method as reference data. The simulations are performed for different wavelengths in the infrared spectral region that are related to specific gas absorption lines. Here both single ZnO nanorods and nanorod arrays with varying period lengths are investigated. The evanescent field distributions and penetration depths into the surrounding media are analyzed and compared as a function of wavelength and rod diameter. Our results give a general overview on the size range where ZnO nanorods may be used for evanescent field interaction based sensors for the detection of gas molecules like CO, CO₂ or O₂.

© 2007 WILEY-VCH Verlag GmbH & Co. KGaA, Weinheim

1 Introduction

Optical waveguides with diameters in the range of ten to hundreds of micrometers have been well studied for many decades and are successfully applied in optical communication and sensing, where, for example, commercial optical fibers are used for evanescent detection of gas species or liquid media [1–5]. Nanotechnology offers the possibility to design subwavelength-diameter waveguiding structures, and thus providing miniaturized low-loss waveguides in the nanometer region. In recent years the guiding properties of silica or silicon nanorods were reported [6, 7], and there are also few reports about the simulation of the mode structure of hexagonal shaped ZnO nanorods [8, 9]. Nanorods or nanowires obviously offer a number of advantages in contrast to standard optical fibers, where diameters are large compared to the wavelength of light. It has been shown that light trapped by a nanorod with subwavelength dimensions can be mainly guided outside the nanorod as evanescent field [6], thus making these devices ideally suited for evanescent field sensors.

The development of a nanorod-based near-infrared (NIR) optical sensor is of interest for monitoring pollutant gases and their concentration using the interaction of an evanescent wave with the ambient gas. Especially the NIR is an attractive wavelength region since vibrational or vibrational-rotational transitions of, for example, oxygen (O₂), carbon monoxide (CO) or carbon dioxide (CO₂) can be stimulated and therefore detected by NIR spectroscopy. A high sensitivity is conventionally realized by optical fibers where a bare core acts as sensing element; here rather long fibers with a large number of internal reflections are essential for efficient interaction [10]. Alternatively, the sensitivity can be increased by adequate chemical sensitive layers [11]. In this context the evanescent field properties of nanorods will combine the advantages of sensitivity by an enhanced evanescent field and a high surface area, and miniaturization.

* Corresponding author: e-mail: s.boerner@pe.tu-clausthal.de, Phone: +49 5323 722370, Fax: +49 5323 723318

ZnO nanorods are perfectly suited for sensor arrays or single nanorod sensors based on evanescent field interaction with surrounding molecules due to their high refractive index even at NIR wavelengths. Furthermore, ZnO nanorods can easily be produced in high crystalline quality, defined size, orientation and arrangement by a simple vapor–liquid–solid (VLS) process [12]. Up to now mainly the photoluminescence properties of ZnO are widely discussed in Ref. [13–16], showing strong band edge photoluminescence in the UV spectral region, and stimulated emission due to the large band gap of ZnO (3.37 eV) and strong binding energy of excitons at room temperature (60 meV). The optical waveguiding characteristics of ZnO nanorods are rarely discussed. Although there exist reports describing hexagonal shaped waveguides in general [8, 9], only little interest was shown for the evanescent field properties and their applicability as an optical sensor medium.

We want to present two possible setups for evanescent field detection with ZnO nanorods. The simulation of the optical properties of a single nanorod is the basis for single nanorod sensors which offer the smallest possible setup. Calculations on single ZnO nanorods at the absorbing wavelengths of O₂ ($\lambda_1 = 761$ nm), CO₂ ($\lambda_2 = 1570$ nm), and CO ($\lambda_3 = 2330$ nm) are performed in the first part of this report. The waveguiding conditions for single mode operation are examined by a dispersion relation diagram. Additionally the penetration depth and the magnitude of the evanescent field are analyzed for the fundamental mode. By examining the influence and interaction of neighbouring nanostructures the applicability of nanorod sensor arrays will be proved. These structures consist of an array of closely packed nanorods, which again has the advantage of small size and in addition a high interaction volume due to the higher surface area.

2 Computational method and constants

The simulations were done with the freely available software package “MIT Photonic Bands” (MPB). Fully-vectorial Eigen modes of Maxwell’s equations with periodic boundary conditions were computed by preconditioned conjugate-gradient minimization of the block Rayleigh quotient in a plane wave basis [17]. The MPB program has been developed for calculation of periodic arrangements of dielectric structures (photonic crystals). Because we first want to compute the properties of single ZnO nanorods we define a two-dimensional cell large enough to make the energy density at the cell boundaries converge to zero around a hexagonal shaped nanorod. The periodic boundary conditions of MPB are well suited to simulate nanorod arrays as the distances between nanorods can easily be defined and expanded to a photonic crystal-like nanorod array. For reference data the Finite Difference Method (FDM) is used. It solves the Helmholtz equations for the transverse magnetic field components. In contrast to the approach used in the MPB software package which simulates Maxwell equations by expanding the field on a plane wave basis this technique defines the refractive index profile on a discrete rectangular grid and the coupled differential equations of the two transverse field components are replaced by coupled difference equations. One drawback of this method is that contours of the hexagonal structure that are not parallel to the lines of the grid are approximated by stair cases. The algorithm used is based on the one given by Lüsse et al. [18].

To simulate the mode structure of a ZnO nanorod a waveguide with hexagonal x – y cross section and an extension infinitely in z -direction is used. The z -direction is set to be the light propagating direction, and coincides with the preferred growth direction and crystalline c -axis of a ZnO nanorod (Fig. 1). The nanorod diameter is defined as shown in Fig. 1. The wavelength dependent ordinary refractive index of ZnO was calculated using the Sellmeier equation [19]:

$$n(\lambda)^2 = A + \frac{B\lambda^2}{\lambda^2 - C} \quad (1)$$

with $A = 2.84$, $B = 0.84$, and $C = 0.101 \mu\text{m}^2$.

Air with a refractive index of $n_{\text{air}} = 1$ acts as the surrounding medium for all calculations.

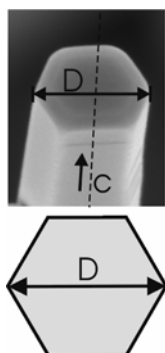


Fig. 1 SEM image (top) and scheme (bottom) of a hexagonal shaped ZnO nanorod with indication of diameter D and crystalline c -axis which coincides with the propagation direction z .

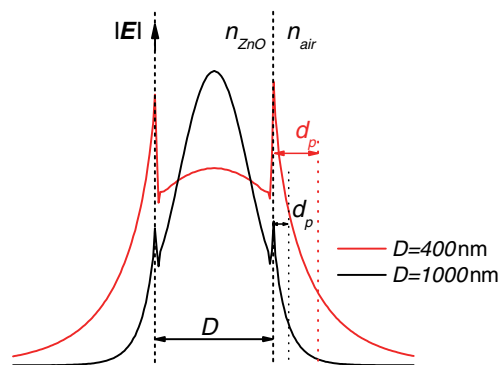


Fig. 2 (online colour at: www.pss-a.com) Scheme of a horizontal cut across the electric field distributions $|E|$ inside and outside a nanorod and the penetration depths d_p for $D = 400$ nm (red) and $D = 1000$ nm (black) at $\lambda_1 = 761$ nm, respectively.

The simulations were performed at three different wavelengths. In future experiments gas molecules of O_2 , CO_2 and CO shall be detected using laser diodes tuned to the respective absorption lines at (vacuum) wavelengths of $\lambda_1 = 761$ nm (O_2), $\lambda_2 = 1570$ nm (CO_2), and $\lambda_3 = 2330$ nm (CO). Since we are interested in waveguides of small diameter and high evanescent field, only the lower modes of ZnO nanorods are computed. The minimal nanorod diameter is assumed to be $D = 20$ nm, so quantum effects have not to be taken into account.

To demonstrate the applicability of ZnO nanorods for evanescent detection of gas molecules two relevant parameters have to be investigated. First single mode condition has to be figured out. For this the dispersion relations are calculated at the gas absorbing wavelengths. Second, the computed electric field is used to obtain the penetration depth d_p of the evanescent field outside the nanorod. This is done to obtain the optimum diameter for both, efficient wave guiding and maximum evanescent field. The penetration depth is set to be the distance between the maximum magnitude of the electric field close to the air-ZnO interface and the position where the field decreases to a value $1/e$ of the initial magnitude. This is illustrated in Fig. 2. The step in the electric field is due to its normal component as the tangential component of E is steady along the interface.

3 Wave guiding properties of single ZnO nanorods

For the development of evanescent field based sensors it is important to determine a reasonable diameter range for single mode operation and a lower limit of stable waveguiding regarding the practical background and possible losses caused by crystalline imperfections. Therefore we computed the mode structure and Eigen frequencies at λ_1 , λ_2 and λ_3 for lower modes. The resulting dispersion relations show the behavior of Δn which is defined as the difference of the effective refractive index n_{eff} and the refractive index $n_{\text{air}} = 1$. n_{eff} is given by the ratio of propagation constant β to vacuum wave number k_0 . From these relations we determine the mono-mode region to an upper value D_2 at which the second mode appears. In Fig. 3 the dispersion relation was simulated for $\lambda_1 = 761$ nm using both the MPB code and FDM. For both methods mode degeneration is clearly seen in this diagram by closely located graphs. For single mode operation it has to be considered that the second mode will appear at a diameter $D_{2(\text{MPB})} = 390$ nm and $D_{2(\text{FDM})} = 360$ nm, respectively. An uncertainty of 5 nm is estimated by a marginal offset of Δn at the given values. An average difference of 30% is observed above D_2 between the values of Δn for the fun-

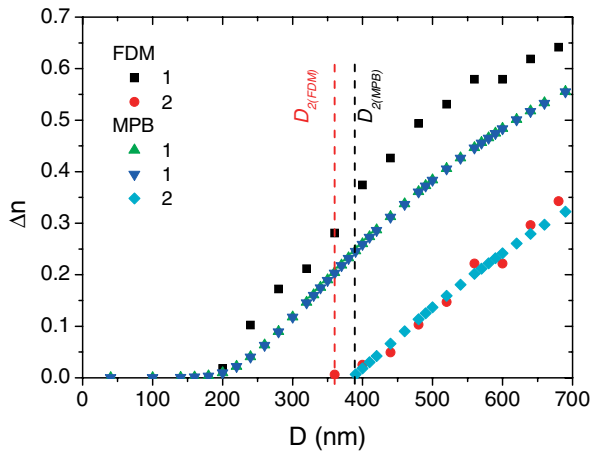


Fig. 3 (online colour at: www.pss-a.com) Dispersion relation $\Delta n(D)$ for a vacuum wavelength of $\lambda_1 = 761$ nm. The upper limit in diameter is indicated by $D_{2(\text{MPB})}$ for the MPB data and $D_{2(\text{FDM})}$ for FDM data.

damental mode calculated by MPB and FDM. These differences may be explained by differing waveguiding selection conditions and the fundamental differences in the simulation procedure, e.g. the discrete grid in FDM.

As mentioned earlier a reduction of the rod diameter will reduce the guided electric field inside and increase the evanescent field outside the rod. This behavior is best shown by the three dimensional plots in Fig. 4 using diameters $D = 300$ nm (a), $D = 600$ nm (b), and $D = 1000$ nm (c). In particular for the smaller diameters a significant part of light is guided outside the nanorod as an evanescent wave.

In a second step the evanescent field was analyzed for the fundamental mode [Fig. 5(a)] using an intersection line across the magnitude of the electric field $|E|$ as illustrated in the inset of Fig. 5(b). Here E_{max} is defined as the maximum magnitude of the evanescent field and situated along the horizontal line at the air-ZnO interface. As expected the normalized value of E_{max} increases with decreasing rod diameter which is due to the redistribution of the field guided inside the rod towards the evanescent field guided outside. A steep decay is observed below the maximum at $D_{\text{MPB}} = 336$ nm (MPB) and $D_{\text{FDM}} = 322$ nm (FDM) [Fig. 5(a)]. MPB method and FDM give similar results, and the obtained diameter D is just slightly differing. The penetration depth d_p is defined by the distance from the ZnO-air interface where the electric field decayed to the value $1/e$. The graph of the electric field of the section plane was fitted outside the hexagonal nanostructure from E_{max} to the cell boundaries, and d_p is calculated for each simulated diameter. The FDM data are slightly different to the MPB calculation, which is mainly caused by the fitting procedure. The resulting curve in Fig. 5(b) shows a super-linear increase for $\lambda_1 = 761$ nm. The penetration depth increases up to about twice the nanorod diameter within the calculated diameter range, which is fundamental for effective evanescent field interaction with a surrounding

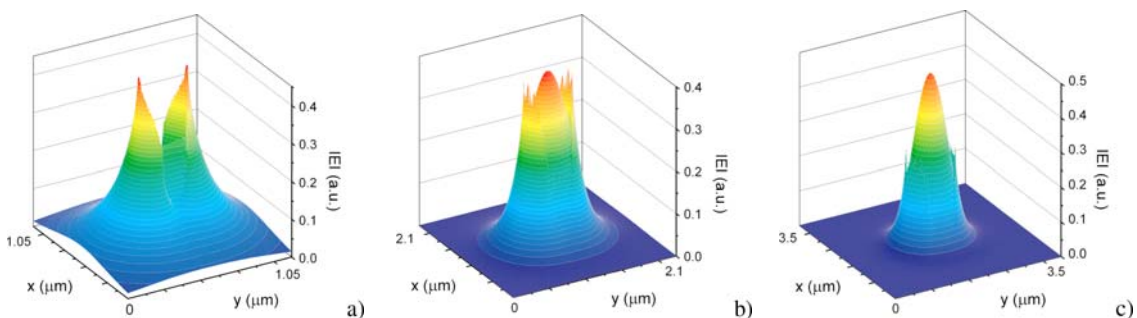


Fig. 4 (online colour at: www.pss-a.com) Three-dimensional model of the absolute value of the electric field $|E|$ of nanorods with diameters (a) $D = 300$ nm, (b) $D = 600$ nm, and (c) $D = 1000$ nm at $\lambda_1 = 761$ nm.

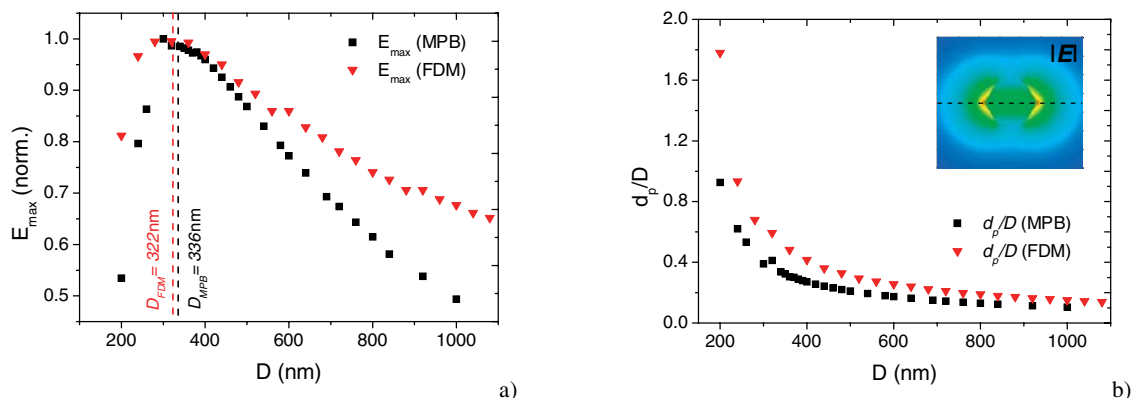


Fig. 5 (online colour at: www.pss-a.com) (a) Normalized maximum magnitude of the evanescent field E_{\max} as a function of rod diameter. (b) Penetration depth obtained by MPB and FDM as a function of diameter for $\lambda_1 = 761$ nm. The inset shows schematically the used cut across the fundamental mode field distribution.

medium. Looking at the penetration depth a small rod diameter obviously offers the largest interaction zone at the expense of a decreasing E_{\max} .

In a first summary, we got two characterizing diameters estimating the efficiency of evanescent field interaction. First the single mode operation is defined by an upper diameter $D_{2(\text{MPB})} = 390$ nm, and second the maximum of evanescent field appears at $D_{\text{MPB}} = 336$ nm. The transition of the electric field of the fundamental mode is illustrated in Fig. 6 beginning with a 200 nm nanorod up to a 390 nm rod at which the single mode criteria ends. The maximum of evanescent field appears at two edges of the hexagon spreading radially towards the cell boundaries while the guided field is elliptical shaped inside the hexagonal structure. The maximum of the evanescent field typically occurs at the corners of the nanorod due to the hexagonal shape. The decrease of the evanescent field outside and the increase of the field inside the nanorod at $D_{2(\text{MPB})}$ is noticeable. Although only a small part of the light is guided inside the dielectric structure at $D = 200$ nm E_{\max} is small and the evanescent field spreading widely outwards. Although there is no lower diameter limiting the waveguiding, the loss of weakly guided modes will play an important role in applications as imperfections in the nanostructure can occur.

The previous calculations at λ_1 were also performed and analyzed for the two other wavelengths λ_2 and λ_3 . Figure 7 shows the results obtained for all the three wavelengths and additional wavelengths lying in between to confirm the progression of the characteristic diameters D_{MPB} and D_{FDM} at E_{\max} , and the upper boundaries $D_{2(\text{MPB})}$ and $D_{2(\text{FDM})}$ for single mode condition when the second mode appears. They are linearly increasing to $D_{\text{MPB}} = 661$ nm and $D_{\text{FDM}} = 694$ nm, and $D_{2(\text{MPB})} = 800$ nm and $D_{2(\text{FDM})} = 660$ nm at λ_2 . The characteristic diameters at λ_3 are $D_{\text{MPB}} = 1008$ nm and $D_{\text{FDM}} = 1033$ nm, $D_{2(\text{MPB})} = 1200$ nm and $D_{2(\text{FDM})} = 1020$ nm, accordingly. The upper diameters of single mode condition $D_{2(\text{MPB})}$ obtained using MPB are slightly above the values of D_{MPB} where the evanescent field has its maximum value. In contrast

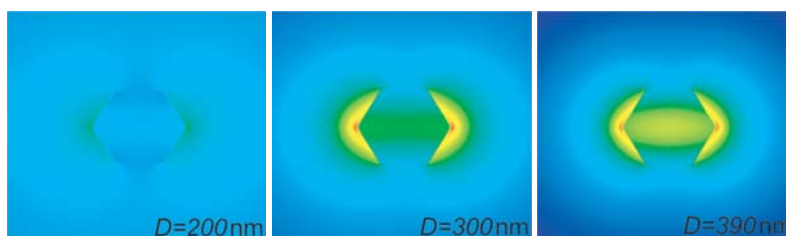


Fig. 6 (online colour at: www.pss-a.com) Evolution of the magnitude of electric field at $\lambda_1 = 761$ nm of $D = 200$ nm, $D = 300$ nm, and $D_{2(\text{MPB})} = 390$ nm.

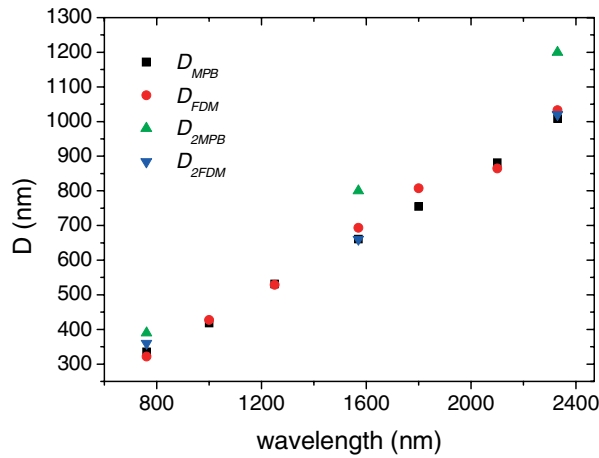


Fig. 7 (online colour at: www.pss-a.com) Characteristic diameters as a function of wavelength for single mode condition ($D_{2(MPB)}$, $D_{2(FDM)}$) and maximum magnitude of evanescent field (D_{MPB} , D_{FDM}).

$D_{2(FDM)}$ and D_{FDM} are very close to each other which allow the presumption that the transition to the next mode is directly following the highest magnitude of evanescent field.

4 Wave guiding properties of ZnO nanorod arrays

In the last section single ZnO nanorods were simulated using the MPB code by increasing the cell size of surrounding air in a way that the energy density at the cell boundary converges against zero. However, MPB offers an easy way to simulate nanorod arrays in a similar way. This is done by decreasing the cell size while the rod diameter is held constant, i.e. increasing the influence of neighboring nanorods. This supports coupling between nanorods and their evanescent fields which will change the Eigen frequencies and values. This increases the effective refractive indexes to allow strong waveguiding in a wider diameter range.

The cell size a was varied from 1- to 40-fold of rod diameter. It is defined by the distance of the centers of two neighboring nanorods arranged in square lattice. For each cell size the effective refractive index of the fundamental mode of the photonic crystal was calculated. The result is shown in Fig. 8(a) for $\lambda_1 = 761$ nm, representatively. Obviously the value Δn stays constant for large distances and rapidly

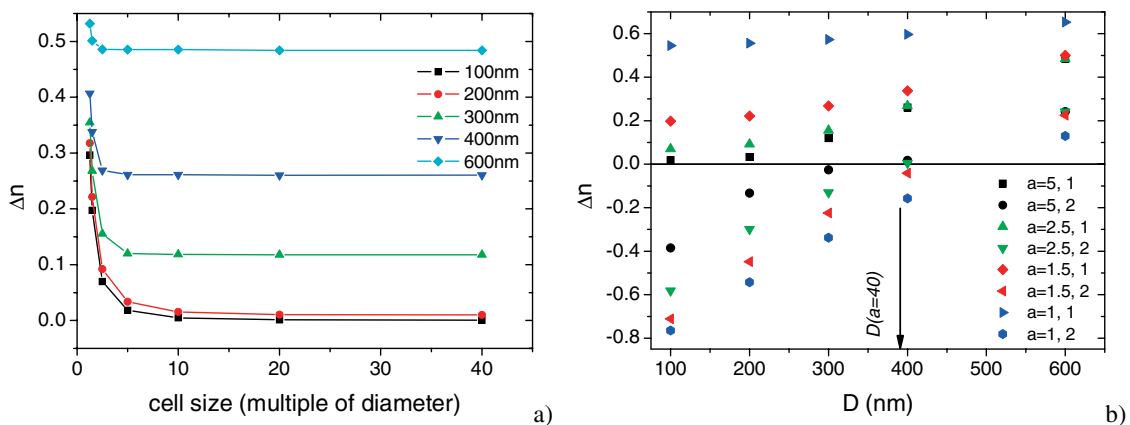


Fig. 8 (online colour at: www.pss-a.com) (a) Evolution of the effective refractive indices of the fundamental modes of different nanorod diameters with cell size. (b) Evolution of the effective refractive indexes of the lowest two modes. The legend gives the computed cell size a in multiples of diameter followed by the mode index.

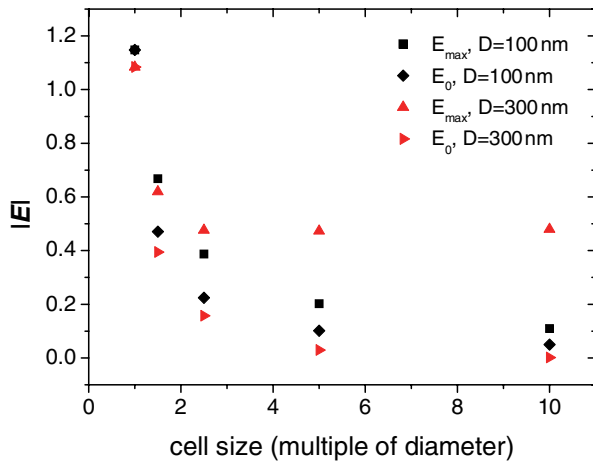


Fig. 9 (online colour at: www.pss-a.com) Magnitude of the value of the evanescent field at its maximum (E_{\max}) and at the cell boundary (E_0) as a function of the cell size.

increases to higher values as the cell size more and more decreases. Figure 8(a) shows a constant progression in a range of 20- to 40-fold of diameter where influences of the periodic array are negligible and a single nanorod can be considered. Subsequently, below a relative cell size of 10 the values of Δn increase super linearly and the model of a single structure has to be replaced by a model for a periodic array. In the case of nanorod arrays this will provide a smaller usable diameter, and at the same time they may form a more stable waveguide device regarding defects or imperfections of single nanorods. The behavior of the effective refractive indices of the fundamental and second mode is shown in Fig. 8(b). Obviously Δn is increasing with decreasing cell size at constant diameter as in Fig. 8(a). Additionally an increase in distance to the second mode is observed as the cell size decreases. This means a shift of $D_{2(\text{MPB})}$ to higher diameters allowing a wider range of single mode condition.

Finally the behavior of the maximum magnitude of the evanescent field close at the nanorod surface (E_{\max}) and the field at the cell boundaries (E_0) is compared in Fig. 9 for 100 nm and 300 nm rods. Both, E_{\max} and E_0 are rapidly increasing when the cell size is decreased and converge to the same value when the edges of the hexagons are in direct contact (cell size is equivalent to diameter). This behavior is represented by the three-dimensional plots in Fig. 10(a) and (b) for an array of 200 nm rods in a 3×3 square alignment. Peaks with the maximum value E_{\max} at the edges of the hexagon are noticeably increasing

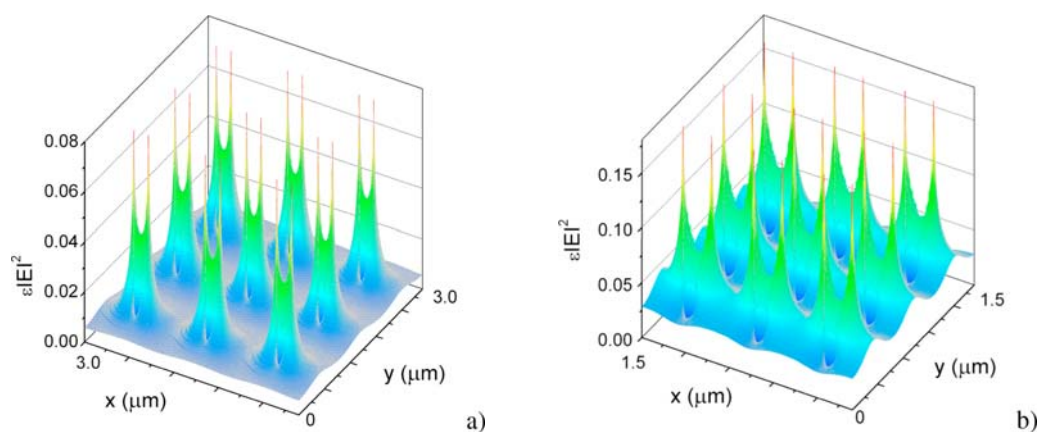


Fig. 10 (online colour at: www.pss-a.com) Three dimensional plots of a 3×3 nanorod array with diameter $D = 200$ nm. (a) Cell size $a = 5$ showing a $3 \mu\text{m} \times 3 \mu\text{m}$ section and (b) cell size $a = 2.5$ showing a $1.5 \mu\text{m} \times 1.5 \mu\text{m}$ section to demonstrate the evolution of electric field inside and outside a nanorod in an array.

when the cell size is decreased. While the evanescent field between neighboring nanorods is nearly decreasing to zero at a cell size of 5, the coupling at $a = 2.5$ results in a raising in-between.

5 Conclusions

We have shown the applicability of ZnO nanorods as optical sensing material using “MIT Photonic Bands” simulation software (MPB) and the Finite Difference Method (FDM). Both methods provided well coinciding results proving the applicability of MPB for single nanorod condition. Especially at small rod diameters MPB is an interesting alternative as the computation of a discrete grid possibly limits the resolution of the hexagonal ZnO nanorod. The main advantage of the MPB software certainly is the simulation of periodic arrays.

Calculations were done for the wavelengths $\lambda_1 = 761$ nm for oxygen, $\lambda_2 = 1570$ nm for carbon dioxide, and $\lambda_3 = 2330$ nm for carbon monoxide being vibrational or vibrational-rotational transitions of those molecules. Two characteristic diameters were figured out by analyzing the dispersion relations and the electric field distributions defining a promising diameter range for efficient evanescent field detection. At $\lambda_1 = 761$ nm the evanescent field has a maximum at $D = 336$ nm (MPB) and $D = 322$ nm (FDM). Because the field is subsequently decreasing the upper diameter limit is set to guarantee single mode condition to $D_{2(\text{MPB})} = 390$ nm and $D_{2(\text{FDM})} = 360$ nm. Accordingly those diameters can be calculated for λ_2 and λ_3 and are obtained to be $D_{\text{MPB}} = 661$ nm and $D_{\text{FDM}} = 694$ nm, and $D_{2(\text{MPB})} = 800$ nm and $D_{2(\text{FDM})} = 660$ nm at λ_2 . The characteristic diameters at λ_3 are $D_{\text{MPB}} = 1008$ nm and $D_{\text{FDM}} = 1033$ nm, $D_{2(\text{MPB})} = 1200$ nm and $D_{2(\text{FDM})} = 1020$ nm. The ratio of the evanescent field to the electric field inside the rod can be increased to values close to one providing a high interaction area around a nanorod.

The setup of a nanorod array is able to change the characteristic diameters by taking advantage of interacting neighboring rods and coupling of evanescent fields. Thus the limit for single mode condition is moving to higher diameters, the quality of waveguiding is increased for small diameters by the increase of the effective refractive index and the maximum magnitude of the evanescent field is increasing with decreasing distances. This was verified for nanorods in rectangular lattices. The main advantage for this kind of application is clearly the enlargement of the interacting zone by having a large amount of nanorods in a small device.

The concept of evanescent field interaction of nanoscale systems is certainly a promising method to adopt for miniaturized optical sensors. We have shown that a nanorod-based evanescent wave sensor is an attractive tool for monitoring pollutant gases. It has to be confirmed experimentally that the theoretical model can be adapted to a real system as crystalline quality, defects or alignment play an important role for the realisation of this sensor concept.

References

- [1] A. R. Lennie and F. Kvasnik, *Anal. Chim. Acta* **281**, 265–270 (1993).
- [2] J. Bürck, J.-P. Conzen, and H.-J. Ache, *J. Anal. Chem.* **342**, 394–400 (1992).
- [3] H. Tai, H. Tanaka, and T. Yoshino, *Opt. Lett.* **12**, 437–439 (1987).
- [4] U. Willer, D. Scheel, I. Kostjucenko, C. Bohling, W. Schade, and E. Faber, *Spectrochim. Acta A* **58**, 2427–2432 (2002).
- [5] U. Willer, M. Saraji, A. Khorsandi, P. Geiser, and W. Schade, *Opt. Lasers Eng.* **44**, 699–710 (2006).
- [6] L. Tong, J. Lou, and E. Mazur, *Opt. Express* **12**, 1025–1035 (2004).
- [7] J. Lou, L. Tong, and Z. Ye, *Opt. Express* **13**, 2135–2140 (2005).
- [8] R. Hauschild and H. Kalt, *Appl. Phys. Lett.* **89**, 123107 (2006).
- [9] T. Nobis and M. Grundmann, *Phys. Rev. A* **72**, 063806 (2005).
- [10] D. S. Blair, L. W. Burgess, and A. M. Brodsky, *Anal. Chem.* **69**, 2238–2246 (1997).
- [11] O. B. Miled, H. B. Ouada, and J. Livage, *Mater. Sci. Eng. C* **21**, 183–188 (2002).
- [12] M. H. Huang, Y. Wu, H. Feick, N. Tran, E. Weber, and P. Yang, *Adv. Mater.* **13**, 113–116 (2001).
- [13] P. Yang, H. Yan, S. Mao, R. Russo, J. Johnson, R. Saykally, N. Morris, J. Pham, R. He, and H.-J. Choi, *Adv. Funct. Mater.* **12**, 323–331 (2002).

- [14] J. C. Johnson, H. Yan, P. Yang, and R. Saykally, *J. Phys. Chem. B* **107**, 8816–8828 (2003).
- [15] L. Wischmeier, C. Bekeny, T. Voss, S. Börner, and W. Schade, *phys. stat. sol. (b)* **243**, 919–923 (2006).
- [16] L. Wischmeier, T. Voss, S. Börner, and W. Schade, *Appl. Phys. A* **84**, 111–116 (2006).
- [17] S. G. Johnson and J. D. Joannopoulos, *Opt. Express* **8**, 173–190 (2001).
- [18] P. Lüsse, P. Stuwe, J. Schüle, and H.-G. Unger, *J. Lightwave Technol.* **12**, 487–494 (1994).
- [19] H. Yoshikawa and S. Adachi, *Jpn. J. Appl. Phys.* **36**, 6237–6243 (1997).